COMPARISON OF HARD SCATTERING MODELS FOR PARTICLE PRODUCTION AT LARGE TRANSVERSE MOMENTUM. I. CONSTRAINTS ON HARD COLLISION CROSS SECTIONS FROM OPPOSITE SIDE RAPIDITY DISTRIBUTIONS

By E.-M. Ilgenfritz, J. Kripfganz*, H.-J. Möhring, Gisela Ranft, J. Ranft and A. Schiller

Sektion Physik, Karl-Marx-Universität, Leipzig**

(Received June 16, 1977; final version received August 16, 1977)

Opposite side rapidity distributions at large $p_\perp$ are analysed using different hard collision models: $qq \to qq$, $q\bar{q} \to M\bar{M}$, $qM \to qM$. We find the hard scattering cross section $d\sigma/d\hat{t}$ to be strongly constrained by the data. Some forms for $d\sigma/d\hat{t}$ proposed previously are found to be inconsistent with the data; but choosing empirical parametrizations all models are able to describe the presently known data. However, at larger trigger transverse momenta we find differences between the models.

1. Introduction

Considerable progress has been made during the last year in the investigation of hadronic reactions at large transverse momentum [1, 2, 3]. The transverse momentum dependence of single particle distributions is now better understood [4, 5]. Correlation measurements give increasing evidence for a two-jet-event-structure [6–11] as predicted by hard collision models.

The explanation of large transverse momentum phenomena by the hard collision of partons has obtained some experimental support but many questions remain to be answered. These questions concern:

(*i*) The distributions and quantum numbers of partons in hadrons;
(*ii*) the distribution functions describing the fragmentation of partons into jets of hadrons;
(*iii*) the hard collision cross section and the nature of constituents which participate in large $p_\perp$ reactions;
(*iv*) properties of the large $p_\perp$ final states like quantum number correlations and jet structure.

* Presently at CERN, Geneva, Switzerland.
** Address: Sektion Physik, Karl-Marx-Universität, Karl-Marx-Platz, 701 Leipzig, DDR.

Preferably, the answers (*i*) and (*ii*) should be obtained from lepton-hadron and lepton--lepton reactions.

In the present paper as in [12], we want to study the questions: What is the correct hard collision model and what is the form of the parton-parton cross section. To this end we analyse data on opposite side two-particle correlations in rapidity. We study hard collision models which were proposed in the past by different groups and which were shown to lead to reasonable agreement with the $p_\perp$ dependence of single particle distributions in pp and $\pi^\pm$p collisions [13–25]. Data on same side and opposite side two--particle correlations [26] as function of transverse momentum were found to agree well to these hard scattering models in a number of papers [27–32]. Same side and opposite side large $p_\perp$ correlations in the rapidity variable within these models were studied in Refs [12, 22, 23, 29, 33–35]. In Section 2 we give details about the hard scattering models considered. We discuss the parton distributions $F_h^q(x)$ in hadrons and the parton fragmentation functions $G_h^q(z)$ as well as the parton-parton cross sections which we will use. In Section 3 we derive constraints on the parton-parton hard collision cross sections from recent data on opposite side rapidity distributions [10]. We extend the results of Kripfganz and Ranft [12] considering additional hard collision models. Indeed we are able to show that some of the hard scattering cross sections $d\sigma/d\hat{t}$ which were proposed in the past are inconsistent with these data. However, choosing $d\sigma/d\hat{t}$ phenomenologically we are able to describe the correlation data in all models considered reasonably well. In Section 4 we present our conclusions and discuss proposals for future experiments.

2. Hard scattering models

2.1. Description of the hard scattering models considered

The general structure of hard scattering models is illustrated in Fig. 1. In the collision of hadrons A and B, secondary hadrons C and D with large transverse momentum are produced via the hard scattering of pointlike constituents, partons i and j. The partons i and j are fragments of the incoming hadrons A and B. $\frac{1}{x_1} F_A^i(x_1)$ and $\frac{1}{x_2} F_B^j(x_2)$ are the

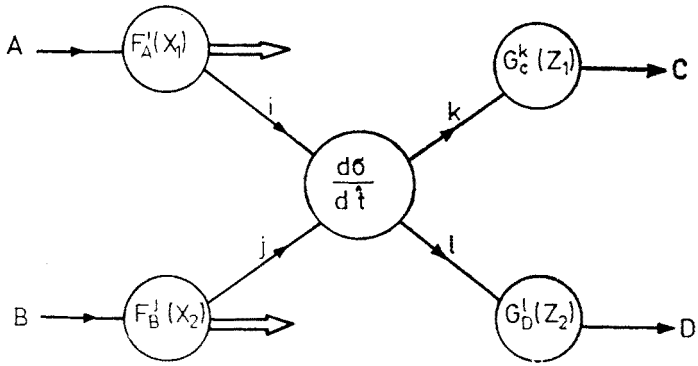

Fig.1. The hard collision model

momentum distributions of partons i and j in the hadrons where x_1 gives the fraction of the hadron momentum carried by the parton i, $x_1 = p_i/P_A$. The scattered partons k and l are usually not directly observed, e.g. if they carry quark quantum numbers. The observed hadrons C and D result from the "decay" of the partons k and l into hadrons. The momentum distributions of hadrons in the parton fragmentation are given by $\frac{1}{z_1} G_C^k(z_1)$ and $\frac{1}{z_2} G_D^l(z_2)$ where $z_1(z_2)$ gives the fraction of the parton momentum carried away by the hadron $C(D)$; $z_1 = p_C/p_k$. Inclusive two-particle distributions according to this picture are given by the following expressions [13, 14]

$$E_C E_D \frac{d^6\sigma}{d^3p_C d^3p_D} \approx \frac{16}{\pi s x_{\perp C}^2 x_{\perp D}^2} \int \frac{x_1 dx_1}{\left(\operatorname{ctg}\frac{\theta_C}{2} + \operatorname{ctg}\frac{\theta_D}{2}\right)^2}$$

$$\times \sum_{i,j,k,l} F_A^i(x_1) F_B^j(x_2) \frac{d\sigma}{d\hat{t}} G_C^k(z_1) G_D^l(z_2). \tag{2.1}$$

The variables $\hat{s}$, $\hat{t}$ and $\hat{u}$ are the Mandelstam variables characterizing the irreducible parton collision. $d\sigma/d\hat{t}$ is the parton-parton hard collision cross section. In Eq. (2.1) the transverse momenta of partons within the hadrons and the transverse momenta of hadrons in the jets resulting from parton fragmentation are neglected. Transverse momenta of hadrons in jets can be taken into account for instance using the methods developed in Refs [33, 34]. This leads to transverse momentum dependent correlation lengths in rapidity for two particles coming both from the same side or opposite side jet and to some increase of the widths of the single particle rapidity distributions and opposite side rapidity distributions. For the purpose of this paper these effects are in most cases neglectable.

Within the general framework of hard scattering models many different models can be considered, which differ mainly in the nature and quantum numbers of the constituents. The aim of our paper is to find from experimental data constraints sufficiently strong to reduce the number of different models which are able to describe the data. We analyse here only opposite side rapidity distributions. In a following paper we analyse the $p_\perp$ and rapidity dependence of single particle distributions and π^+/π^- ratios. The models considered are characterized by the following irreducible subcollisions:

A. Quark-quark elastic scattering, see Fig. 2a. The constituents i and j are the quarks u, d, s and antiquarks $\bar{u}$, $\bar{d}$, $\bar{s}$ in the hadrons [13–17].

B. Quark-antiquark fusion into mesons, see Fig. 2b. The constituents i are quarks u, d, s and the constituents j are antiquarks $\bar{u}$, $\bar{d}$, $\bar{s}$. The outgoing particles k and l carry meson quantum numbers consistent with each other, with the incoming quarks and antiquarks as indicated by the quark lines in Fig. 2b [24, 25].

C. The constituent interchange model, quark + meson → meson + quark, see Fig. 2c. The constituents j and k are quarks u, d, s or antiquarks $\bar{u}$, $\bar{d}$, $\bar{s}$, the constituents i and l

are mesons with quantum numbers consistent with each other and the quarks j and k, as indicated by the quark lines in Fig. 2c [18, 19, 20].

D. Quark-meson scattering with gluon exchange, see Fig. 2d. The constituent i is a quark or an antiquark, j carries meson quantum numbers.

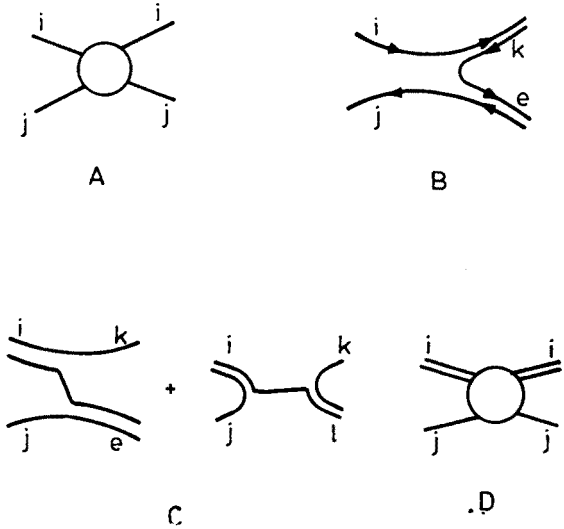

Fig. 2. The four hard collision models considered A — qq → qq, B — $q\bar{q}$ → $M\bar{M}$, C — qM → Mq (CIM), D — qM → qM (gluon exchange)

We consider two versions of each of the models B, C and D, where mesons participate in the hard collision process.

(*i*) The trigger meson might be one of the directly produced unfragmented mesons.

(*ii*) The trigger meson is the product of the fragmentation of constituents with meson or quark quantum numbers. The fraction of observed not fragmenting trigger mesons is enhanced by the trigger bias in the usual experiments [26–32].

2.2. Parton distributions in hadrons

For models A, B, C and D the quark and antiquark distributions in hadrons are needed. For models C and D we need in addition the distribution of meson constituents in hadrons. We use the momentum distribution of partons i in a hadron A in the form

$$P_A^i(x) = \frac{1}{x} F_A^i(x). \tag{2.2}$$

The distributions of quark-partons in hadrons can be determined experimentally in deep inelastic lepton-hadron scattering experiments. The present knowledge of these functions is, however, not satisfactory.

The distributions of quarks and antiquarks in protons and neutrons were extracted in many papers from deep inelastic scattering data [15, 38–44]. In these papers also sum

rules and constraints are discussed and exploited to get realistic distributions. In our actual calculations we use the distributions proposed by Barger and Phillips [39] and the ones due to McElhaney and Tuan [38] It is to be recognized that distributions available so far are subject to large uncertainties. It is known experimentally from eN, μN and νN collisions [45] that scaling in the variable x is violated. The data from muon and neutrino collisions at higher energies than the SLAC data give, however, not yet a coherent picture. Therefore we use for the time being the distributions with exact scaling. With a few exceptions the rapidity distributions which we calculate are rather insensitive to the exact shape of the quark distributions depending more sensitively on the hard scattering cross section. The distributions of sea quarks are particularly ill defined from present data. McElhaney and Tuan [38] fit the sea distribution as

$$P_A^s(x) = \frac{1}{x} s(x); \quad s(x) = 0.1(1-x)^{7/2}. \tag{2.3}$$

Barger and Phillips [39] propose

$$s(x) = 0.145\,(1-x)^9. \tag{2.4}$$

The dimensional counting rules give [44]

$$s(x) \sim (1-x)^7. \tag{2.5}$$

We perform many of our calculations, in particular when using the quark-antiquark fusion model B, using both of the distributions (2.3) and (2.4). In this way we hope to get a feeling for the uncertainties of the calculated large $p_\perp$ cross sections due to the uncertainties in the quark distribution functions.

The quark distributions in mesons are not available from lepton induced reactions. We use in our calculations distributions as suggested by dimensional counting arguments [41]. For instance for π^+, these distributions are of the form

$$F^{u}_{\pi^+}(x) = F^{\bar{d}}_{\pi^+}(x) = 2x(1-x)+0.2(1-x)^5, \tag{2.6}$$

$$F^{d}_{\pi^+}(x) = F^{\bar{u}}_{\pi^+}(x) = F^{s}_{\pi^+}(x) = F^{\bar{s}}_{\pi^+}(x) = 0.2(1-x)^5. \tag{2.7}$$

Finally there remain the pion distributions in hadrons needed for models C and D. These distributions are again very ill defined. We use dimensional counting arguments to determine the shape of these distributions.

2.3. Parton fragmentation into hadrons

We use the momentum distributions of hadrons C from the decay of the parton i in the form

$$P_C^i(z) = \frac{1}{z} G_C^i(z), \tag{2.8}$$

where z is the fraction of parton momentum carried by the hadron C, $z = p_C/p_i$.

The fragmentation of quark-partons into hadrons can be studied experimentally in deep inelastic lepton-hadron collisions and in e^+e^- annihilation into hadrons [46, 51]. Here we are mainly concerned with the decay of quarks u and d and antiquarks $\bar{u}$ and $\bar{d}$ into pions. We use for the fragmentation of the u quark into pions the following distributions which were obtained from a chain decay model restricted to pions as secondaries [52]

$$G^u_{\pi^+}(z) = \tfrac{2}{3} - \tfrac{4}{15} z - \tfrac{2}{5} z^{5/3}, \tag{2.9}$$

$$G^u_{\pi^-}(z) = \tfrac{2}{3} - \tfrac{16}{15} z + \tfrac{2}{5} z^{8/3}, \tag{2.10}$$

$$G^u_{\pi^0}(z) = \tfrac{2}{3} - \tfrac{2}{3} z. \tag{2.11}$$

For a comparison with muo and neutrino production data see Fig. 3. These distributions satisfy isospin and energy sum rules. The corresponding distributions for d, $\bar{u}$ and $\bar{d}$ quarks

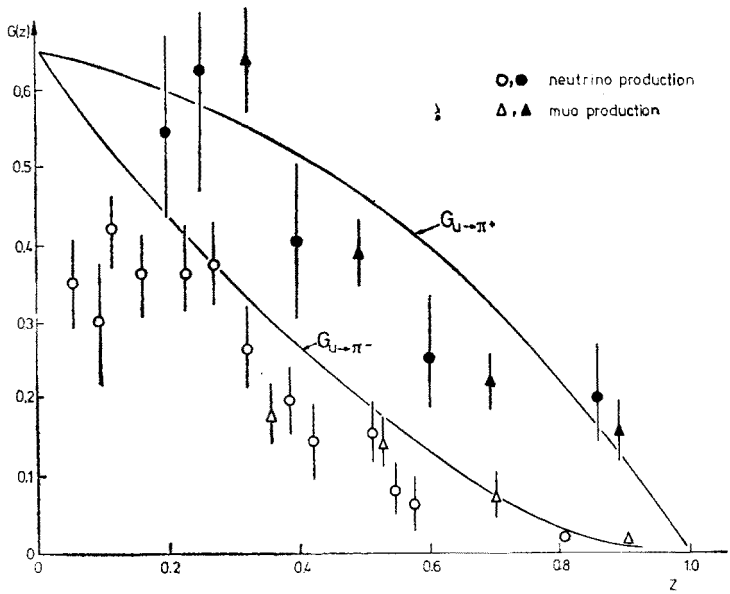

Fig. 3. Comparison of our parametrization of the quark fragmentation function, Eqs (2.9) and (2.10) with data from lepton hadron collisions [50]

are obtained from isospin invariance. The distributions for s and $\bar{s}$ quarks are chosen according to the assumption that all distributions for unfavoured decays like $u \to \pi^-$, $d \to \pi^+$, $s \to \pi^\pm$ etc. are identical [15].

In the fragmentation of meson constituents i into mesons C we choose the momentum distributions of C in the form [27]

$$P^i_C(z) = \frac{1}{z} G^i_C(z) + K\delta_{iC}\delta(1-z), \tag{2.12}$$

where the parameter K determines the fraction of not-fragmenting mesons. This fraction is small [27]. Therefore we consider the not-fragmenting term only for the trigger pion,

where this term is favoured by the trigger bias. As discussed above we calculate the two contributions with fragmenting and non-fragmenting meson constituents separately. We use functions $G_C^i(z)$ for the fragmentation of mesons into mesons as obtained from dimensional counting arguments.

2.4. Parton-parton hard scattering cross sections

The parton-parton cross section is assumed usually to be of the form

$$\frac{d\sigma}{dt} \approx \frac{1}{\hat{s}^n} f\left(\frac{\hat{t}}{\hat{s}}\right) \tag{2.13}$$

motivated by the dimensional counting rules [36, 37]. The experimental behaviour of single particle distributions at large transverse momenta demands $n \approx 4$. The originally

TABLE I

Parton-parton hard collision cross sections considered for various hard collision models

Hard collision model	$\frac{d\sigma}{d\hat{t}} \approx \frac{1}{\hat{s}^4} f\left(\frac{\hat{t}}{\hat{s}}\right)$	$f\left(\frac{\hat{t}}{\hat{s}}\right) = g(\eta)$	Remarks and references
A: $qq \to qq$	$\approx \frac{1}{\hat{s}^4} \frac{(\hat{s}^2+\hat{u}^2)\hat{s}^2}{\hat{t}^4}$ (A.1)	$\left[\left(1+\frac{1}{\eta}\right)^2 + \frac{1}{\eta^2}\right]\left(1+\frac{1}{\eta}\right)^2$	[15] quark form factors
	$= \frac{1}{\hat{s}^4} \frac{\hat{s}^3}{(-\hat{t})^3} \cdot 2.3 \cdot 10^6$	$\left(1+\frac{1}{\eta}\right)^3$	[23] preferred by [15]
	μb GeV^6 (A.2)		
	$\approx \frac{1}{\hat{s}^4} \frac{\hat{s}^2}{(-\hat{t})^2}$ (A.3)	$\left(1+\frac{1}{\eta}\right)^2$	[15]
	$\approx \frac{1}{\hat{s}^4} \frac{\hat{s}^2+\hat{u}^2}{\hat{t}^2}$ (A.4)	$\left(1+\frac{1}{\eta}\right)^2 + \frac{1}{\eta^2}$	[23]
B: $q\bar{q} \to MM$	$\approx \frac{1}{\hat{s}^4} \frac{\hat{s}^3}{(-\hat{t})^3}$ (B.1)	$\left(1+\frac{1}{\eta}\right)^3$	[35]
C: $qM \to qM$	$\approx \frac{1}{\hat{s}^4}\left(\frac{\hat{s}^2}{\hat{u}^2}+1\right)$ (C.1)	$(1+\eta)^2+1$	[23]
	$\approx \frac{1}{\hat{s}^4} \frac{\hat{s}^3}{(-\hat{u})^3}$ (C.2)	$(1+\eta)^3$	[19]
Empirical parametrization for all models	$\frac{1}{\hat{s}^4} f\left(\frac{\hat{t}}{\hat{s}}\right)$	$g(\eta)+g\left(\frac{1}{\eta}\right) = \left(a+\eta+\frac{1}{\eta}\right)^N$	[12]

proposed mechanism [13, 14], quark-quark scattering via gluon exchange, gives $n = 2$ and does not agree with experiment. When considering the mechanism A: qq → qq we do not consider the many possible forms for $d\sigma/d\hat{t}$ discussed by Ellis and Kislinger [14], instead we use quark-quark scattering cross sections introduced phenomenologically as in Refs. [12, 15, 16, 17, 23] with the power $n = 4$ demanded by data. In Table 1 we collect some forms of $d\sigma/d\hat{t}$ considered before in the literature. In Section 3 in which opposite side correlations are analysed we shall discuss which of these cross sections are consistent with correlation data. For most of our applications we use the parametrization proposed in Ref. [12]

$$\frac{d\sigma}{d\hat{t}} = \frac{1}{\hat{s}^4}\, g(\eta), \quad \frac{d\sigma}{d\hat{u}} = \frac{1}{\hat{s}^4}\, g\left(\frac{1}{\eta}\right), \quad \eta = -\frac{\hat{t}/\hat{s}}{1+\hat{t}/\hat{s}}, \tag{2.14}$$

$$g(\eta) + g\left(\frac{1}{\eta}\right) = \left(a+\eta+\frac{1}{\eta}\right)^N, \quad a > 0, \tag{2.15}$$

where a and N are parameters to be determined from the data. According to (2.15), $g(\eta)$ is defined by taking all terms $\left(\frac{1}{\eta}\right)^m$, $m > 0$ and half of the term with $m = 0$,

$$g(\eta) = \frac{c_0}{2} + \sum_{j=1}^{N} c_j \left(\frac{1}{\eta}\right)^j \tag{2.16}$$

with

$$c_j = \sum_{k=0}^{\text{integer}\left(\frac{N-j}{2}\right)} \frac{N!}{(N-2k-j)!(k+j)!k!}\, a^{N-2k-j}. \tag{2.17}$$

The term with $\left(\frac{1}{\eta}\right)^N$ dominates. We use the parametrization (2.15) for all models A, B, C, D considered. In the models B, C and D the dimensional counting rules give for meson production the power $\hat{s}^{-4}$ as demanded by experiment.

2.5. Opposite side two-particle distributions

The opposite side two-particle distributions are calculated according to Eq. (2.1). The detailed structure of these expressions depends, however, on the particular hard scattering model considered, see Fig. 2.

3. Comparison of calculated opposite side rapidity correlations with data

In this Section we want to constrain the parton-parton hard collision cross sections comparing with data on opposite side rapidity distributions. Data on opposite side rapidity distributions were recently published by the CCHK collaboration [10]. The trigger $x_\perp$ is about $x_{\perp 1} = 0.1$, the trigger angles are $\theta_1 = 20°$ ($y_1 = 1.6$) and $\theta_1 = 45°$ ($y_1 = 0.8$).

In our analysis we use only the data for $p_{\perp 2} > 1$ GeV/c, negatively charged trigger and negatively charged opposite side particles. We hope that leading particle effects will be minimal in this channel. Furthermore, we compare only the shape of the calculated opposite side distribution with the shape of the data. As also known from the $d\sigma/dx_e$ distributions, there are problems with absolute normalization of the opposite side distribution in all models. The normalization of the calculated curve is slightly too big. Remedies proposed are superposition of fragmenting (f) and non-fragmenting (nf) mesonic states [27], deviations from scaling of the jet fragmentation functions $G(z)$ [28], invariant masses of jets [31] and transverse momenta of partons in hadrons and hadrons in jets. We do not want to study this question any further here.

The constraints on hard scattering cross sections follow from the shape of the distribution, only. The remarkable feature of the data is the stability of the maximum of the opposite side distribution at $y_2 = 0$ for $x_{\perp 1} \approx 0.1$ irrespective of the trigger rapidity y_1. The appearing picture of opposite side correlations results from the cooperation of different effects:

— dominance of low subenergies in the constituent subcollision; this tends to produce back-to-antiback ($y_1 \cdot y_2 > 0$) correlations;
— relatively broad rapidity distribution of the subcollision c. m. s. in case of unsymmetric constituent collisions (i. e. qM → qM or $q\bar{q} \to M\bar{M}$, where q is valence and $\bar{q}$ is sea quark); this tends to produce double bump structures for trigger $y_1 \approx 0$;
— peripherality of the subcollision differential cross section which has to compensate the effect of low subenergies in view of the experimentally established stability of the associated rapidity distribution with respect to trigger angle (rapidity) at low $x_{\perp 1}$;
— allowing the trigger side jet to fragment, or going to higher trigger $x_{\perp 1}$ gives effectively larger $x_\perp$ to the jet; this tends to produce more back-to-back correlations and more sharply collimated opposite side angular (rapidity) distributions.

3.1. Analysis of opposite side rapidity distributions

We compare the data for negative trigger and negative secondaries [10] with our calculation for $pp \to \pi^-\pi^-X$ at $\sqrt{s} = 53$ GeV. In Figure 4 we compare the data for $y_1 = 1.6$ and $x_{\perp 1} = 0.1$ with three models. Fig. 4a shows the result of a quark-quark scattering model with quark form factors [15] modifying the gluon exchange cross section (Table I, A. 1). The resulting cross section is much too peripheral which shows up in strong back-to-back structure. We have checked that this feature is shared by models with the same leading power $N = 4$ in both η and $1/\eta$. Therefore all attempts to accomodate the $p_\perp^{-8}$ behaviour by modifying structure functions [16] or amplitudes [17] by quark form factors fail. These models give too strong peripherality. In Fig. 4b we find the qM → Mq with the hard collision cross section (C.1 in Table I) originally proposed in CIM to be not peripheral enough, giving strong back-antiback structure. This conclusion differs from the one in [23] where the data of Ref. [10] were not yet available. This qualitatively wrong behaviour is independent of the particular constituent interchange picture. When quark-quark scattering is parametrized in a similar way (Table I, A.3) we find the same correlation pattern (Fig. 4c). Therefore we blame the wrong leading power $N = 2$ for the failure

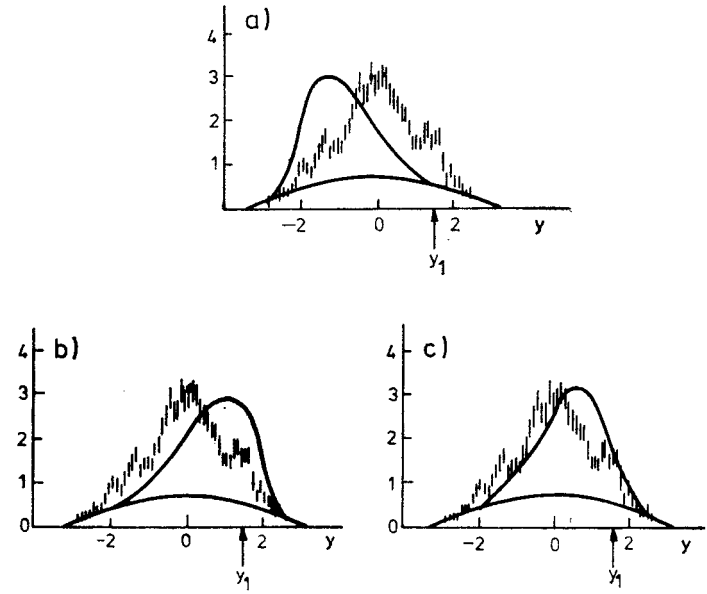

Fig. 4. π^- rapidity distributions for $p_{\perp 2} \geqslant 1$ GeV/c opposite to a π^- trigger at $y_1 = 1.6$ and $x_{\perp 1} = 0.1$ in $pp \to \pi^-\pi^- X$ at $\sqrt{s} = 53$ GeV [10] compared to calculations using models: a) $qq \to qq$ by gluon exchange modified by quark form factors (Table I, A.1), b) $qM \to Mq$ (CIM) (Table I, C.1), c) $qq \to qq$ with phenomenological cross section (Table I, A.3)

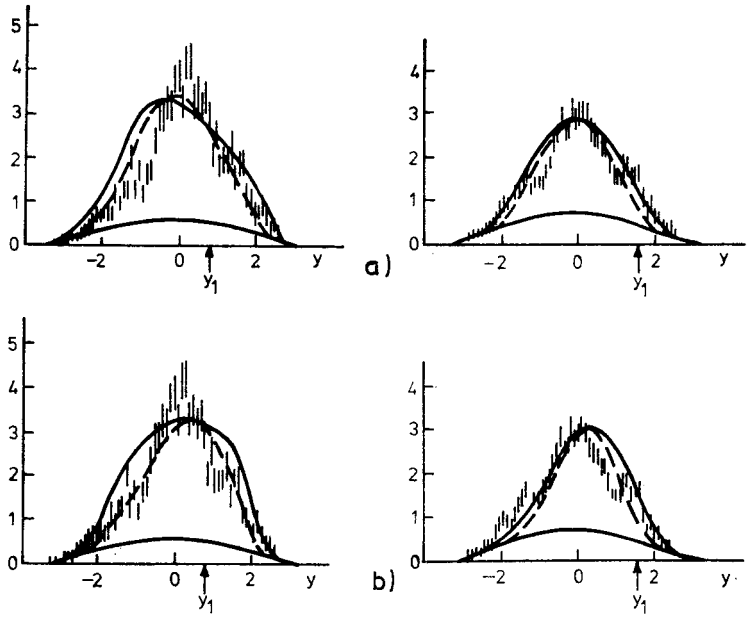

Fig. 5. Same as Fig. 4 for both trigger rapidities $y_1 = 0.8$ and $y_1 = 1.6$ ($\theta_1 = 45°$ and 20°) compared to $qq \to qq$ models using a) phenomenological cross section (2.15) with $a = 1$ and $N = 3$, b) phenomenological cross section (A.2) from Table I

of both models. The 20° data can be successfully described with all models A to D defined in Fig. 2 using the empirical parametrization [12] of the hard collision cross sections defined in (2.14) to (2.16) with the leading power $N = 3$. The same is true with the cross section proposed by Field and Feynman [15] (see Table I, A.2). The leading term in these parametrizations is $\frac{d\sigma}{d\hat{t}} \sim \frac{1}{\hat{s}\hat{t}^3}$. The parameter a in (2.15) controls further the amount of peripherality introduced with $N = 3$. The best agreement with data is reached with $a = 1$ for the qq → qq process and $a = 0.5$ for all other subprocesses.

In Fig. 5 to 7 we show the data [10] with trigger at $x_{\perp 1} = 0.1$ and at both $y_1 = 0.8$ ($\theta_1 = 45°$) and $y_1 = 1.6$ ($\theta_1 = 20°$) in pp collisions at $\sqrt{s} = 53$ GeV and compare them

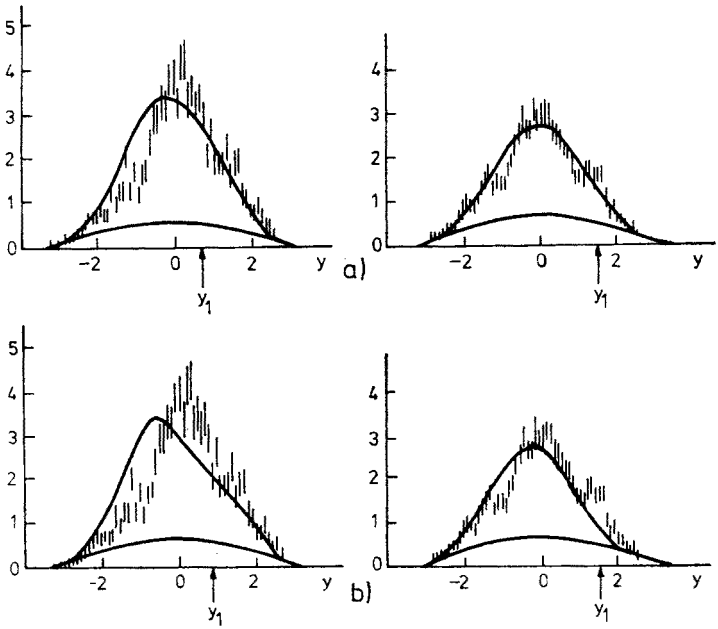

Fig. 6. Same as Fig. 4 for both trigger rapidities $y_1 = 0.8$ and $y_1 = 1.6$ ($\theta = 45°$ and 20°) compared to $q\bar{q} \to MM$ models using a) cross section (2.15) with $a = 0.5$ and $N = 3$, and quark distributions from Ref. [38], b) cross section as in a) and quark distributions from Ref. [39]. Solid curves show distributions with unfragmented trigger meson, dashed ones are distributions when the trigger side jet is required to fragment

with models A ... D. Only the cross sections with acceptable angular dependence mentioned above are considered.

From our comparison of models A ... D with $\pi^-\pi^-$ correlation data we can draw up to now no final conclusions in favour or against any one of the subprocesses involved. But for each model A ... D we may make a best choice:

a) for quark-quark scattering we prefer a phenomenological cross section [12] with the form of Eq. (2.15) (with $a = 1$, $N = 3$) over that of Field and Feynman [15] (Table I, A.2);

b) for quark-antiquark fusion into two meson states we would prefer models with mesonic jets, the empirical cross section (2.15) (with $a = 0.5$, $N = 3$), and Barger-Phillips quark distributions;

c) for quark-meson scattering due to quark exchange we prefer the model version with the same empirical cross section as for b) and with the trigger being the unfragmented meson;

d) for quark-meson scattering due to gluon exchange a model version with the cross section as for b) and with meson constituents fragmenting is in best shape.

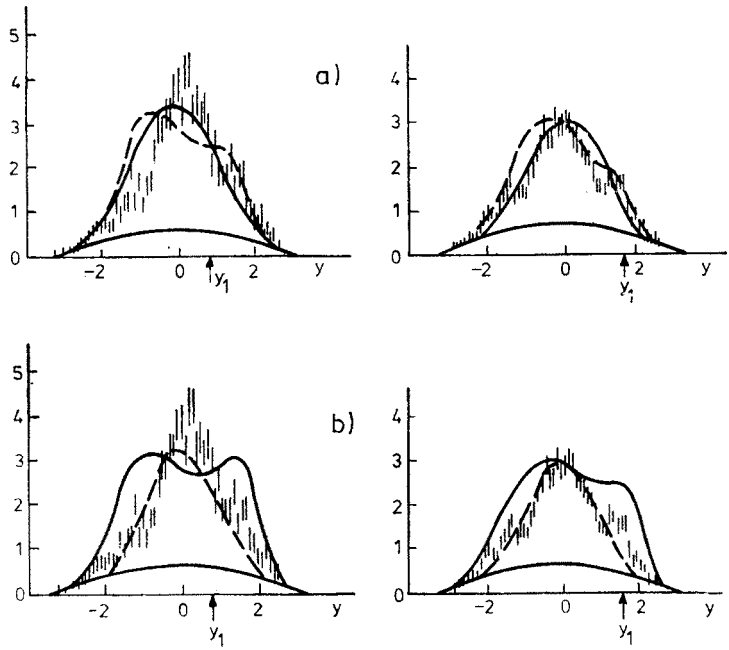

Fig. 7. Same as Fig. 4 for both trigger rapidities $y_1 = 0.8$ and $y_1 = 1.6$ ($\theta_1 = 45°$ and 20°) compared to qM → qM models using the phenomenological cross section (2.15) with $a = 0.5$ and $N = 3$ for a) quark exchange, b) gluon exchange. Solid curves show distributions with unfragmented trigger meson, dashed ones are distributions when the trigger side jet is required to fragment

In either case the 45° data turned out to be most constraining the model version. Models with mesonic constituents which are acceptable only when the trigger particle comes from mesonic jet fragmentation are less probable due to trigger bias.

3.2. $\pi^-\pi^-$ correlations at larger trigger $x_{\perp 1}$ predicted for pp, $\bar{p}p$ and π^-p collision

Extending the analysis of angular correlations at large $p_\perp$ to higher trigger $x_\perp$, other initial states than pp and to other triggers or meson pairs provides predictions perhaps able to discriminate further between subprocesses. We continue to analyse $\pi^-\pi^-$ correlations and show in Fig. 8 predictions of the best version of each model A ... D (selected

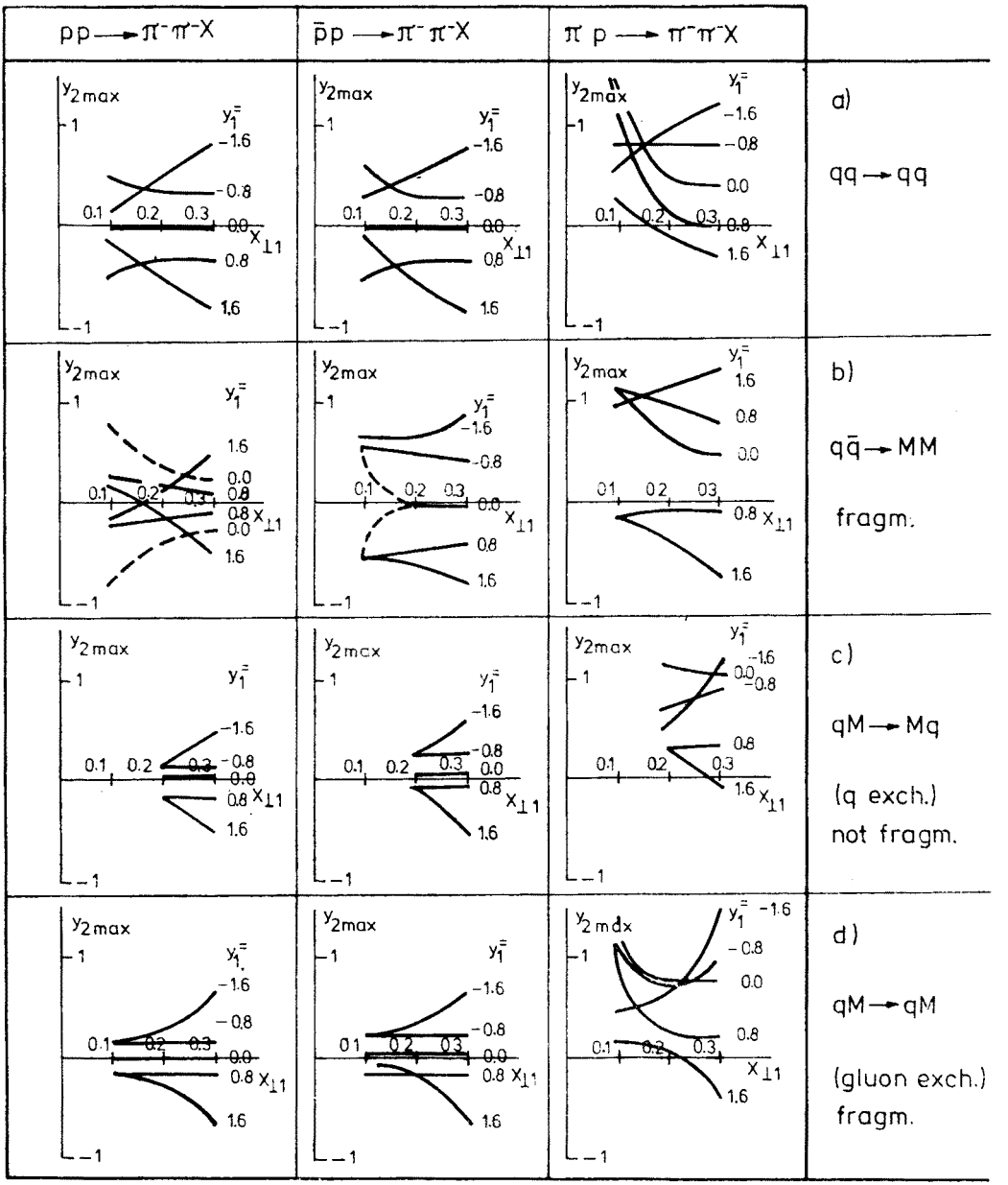

Fig. 8. Predicted maximum position $y_{2\max}$ of the π^- distribution for $p_{\perp 2} \geqslant 1$ GeV/c opposite to a π^- trigger versus trigger $x_{\perp 1}$ (at 0.1, 0.2, 0.3; the curves are drawn to guide the eye) for different trigger rapidities $y_1 = 1.6, 0.8, 0.0, -0.8, -1.6$ or trigger angles $\theta_1 = 20°, 45°, 90°, 135°, 160°$ with respect to the beam for pp, $\bar{p}$p, π^-p collisions at $\sqrt{s} = 20$ GeV from the following models a) qq → qq ($a = 1$, $N = 3$), b) q$\bar{q}$ → MM ($a = 0.5$, $N = 3$) with fragmented trigger, c) qM → Mq ($a = 0.5$, $N = 3$) q exchange, not fragmented trigger, d) qM → qM ($a = 0.5$, $N = 3$) gluon exchange, fragmented trigger. The cross section (2.15) is used in either case. Dashed curves denote double maxima well separated by a dip

in Section 3.1) for pp, $\bar{p}p$ and π^-p collisions at $\sqrt{s} = 20$ GeV. The maximum position $y_{2\max}$ of the ($p_{\perp 2} \geqslant 1$ GeV) rapidity distribution opposite to the π_1^- trigger is shown versus trigger $x_{\perp 1}$ for different trigger angles (y_1) and the three reactions. Opposite side distributions having two maxima opposite to a 90° trigger at low $x_{\perp 1} \approx 0.1$ predicted in the quark fusion model (Fig. 8b) are marked by dashed curves.

In general we see in all models the tendency to strong back-to-back configurations increasing with trigger $x_{\perp 1}$ for $\theta_1 = 20°$ ($y_1 = 1.6$), mainly of kinematical origin, both in pp and $\bar{p}p$ collisions. With respect to $x_{\perp 1}$ the maximum $y_{2\max}$ for $y_1 = 0.8$ ($\theta_1 = 45°$) remains relatively stable in slight back-to-back position, which is a common feature of all models considered except the quark-antiquark fusion model. Only the latter one is able to predict back-antiback correlations at $\theta_1 = 45°$ in $pp \to \pi^-\pi^-X$ but they do not depend on trigger $x_{\perp 1}$. (Even for $\theta_1 = 20°$ we see a back-antiback effect for $x_{\perp 1} < 0.15$). The correlation patterns for pp and $\bar{p}p$ collisions do not differ essentially for all models except quark-antiquark fusion. The reason for this coincidence is that in $qq \to qq$ and $qM \to qM$ processes quarks and antiquarks are involved a priori on equal footing. For the $q\bar{q} \to M\bar{M}$ subprocess the opposite side maxima in $\bar{p}p \to \pi^-\pi^-X$ are well separated in back-to-back position, no crossing occurs. There is no reason for back-antiback correlations according to our qualitative explanation since q and $\bar{q}$ are both valence quarks in p and $\bar{p}$, respectively. The broad double bump structure for trigger $\theta_1 = 90°$ in pp shrinks when changing to $\bar{p}p$ collisions for the same reason, it is less pronounced but still present.

Crossing of the maximum position for $\theta_1 = 20°$ and 45° ($y_1 = 1.6$ and 0.8) before going to small $x_{\perp 1} \approx 0.1$ is a distinguishing feature of quark-quark scattering models. If $\pi^-\pi^-$ back-to-back correlations would be seen in both pp and $\bar{p}p$ collisions this feature could help to discriminate between $qq \to qq$ and $qM \to qM$ models while $q\bar{q} \to M\bar{M}$ would be ruled out.

The $\pi^-\pi^-$ correlation pattern of pp or $\bar{p}p$ collision is shifted forward and distorted for π^-p reactions. The quark-antiquark fusion model is distinguished by the property that only for this process there is still back-to-back correlation possible (in c. m. s. as long as trigger angle $\theta_1 \lesssim 45°$) also for small trigger $x_{\perp 1}$. The other models are not so qualitatively different in their predictions concerning $\pi^-p \to \pi^-\pi^-X$.

4. Conclusions

In this paper we have tried to constrain hard scattering models by comparison of opposite side rapidity distributions with data. We have restricted ourselves to $\pi^-\pi^-$ correlations (negative trigger, negative secondaries) in pp collisions at $\sqrt{s} = 53$ GeV [10]. Comparison at trigger angle $\theta_1 = 20°$ has proven to be restrictive to find the acceptable peripheral behaviour of the hard scattering cross section. Some theoretically motivated cross sections can be eliminated by this check. The proper amount of peripherality and isotropy seems to be represented by our empirical cross section

$$\frac{d\sigma}{d\hat{t}} + \frac{d\sigma}{d\hat{u}} \sim \frac{1}{\hat{s}^4}\left(a + \eta + \frac{1}{\eta}\right)^N, \quad N = 3 \tag{4.1}$$

with the optimal parameter a depending on the type of subprocesses, $qq \to qq$, $q\bar{q} \to M\bar{M}$, or $qM \to qM$ by quark or gluon exchange. The best agreement with the power $N = 3$ (typical also for the quark scattering model of Field and Feynman [15] and certain versions [35] of the quark-antiquark fusion model) signifies dominance of the cross section $\frac{d\sigma}{d\hat{t}} \sim \frac{1}{\hat{s}\hat{t}^3}$. Details like the parameter a in Eq. (4.1) are less influential for the resulting correlation pattern. The choice of the quark distribution functions (Ref. [38] or [39]) is not essential for the correlations except in the quark-antiquark fusion model where some features like e. g., the back-antiback effect at low $x_{\perp 1} \lesssim 0.1$ are sensitively dependent on the amount of kinematical disfavouring of antiquarks within protons. These effects disappear (or decrease) when $\bar{p}p$ reactions instead of pp are considered.

Models which are acceptable only with fragmenting trigger side mesonic state might have problems because of trigger bias which emphazises quasi exclusive trigger.

We conclude that from present data no particular subprocess can be safely excluded. The elimination of certain models should be possible as emphasized in [12] by correlation measurements using identified trigger particles or, as discussed in Section 3.2 by extending the correlation measurements to higher trigger transverse momenta and to different primary beams.

REFERENCES

[1] P. Darriulat, Rapporteur talk given at the 18-th Internat. Conf. on High Energy Physics, Tbilisi, CERN preprint 1976.

[2] M. Della Negra, Review talk given at the VII-th Internat. Colloquium on Multiparticle Reactions, Munich 1976, CERN preprint CERN/EP/Phys. 76–52.

[3] P. V. Landshoff, Invited talk given at the VII-th Internat. Colloquium on Multiparticle Reactions Munich 1976, CERN preprint TH 2227

[4] D. Antreasyan et al., *Phys. Rev. Lett.* **38**, 112 (1977).

[5] D. Antreasyan et al., *Phys. Rev. Lett.* **38**, (1977).

[6] P. Darriulat et al., *Nucl. Phys.* **B107**, 429 (1976).

[7] K. Eggert et al., *Nucl. Phys.* **B98**, 73 (1975).

[8] R. Kephart et al., *Phys. Rev.* **D14**, 2909 (1976).

[9] M. Della Negra et al., CERN–College de France–Heidelberg–Karlsruhe collaboration, CERN preprint CERN/EP/Phys. 76–35, 1976.

[10] M. Della Negra et al., CERN–College de France–Heidelberg–Karlsruhe collaboration, CERN preprint CERN/EP/Phys. 76–43, 1976.

[11] R. Sosnowski, Invited talk given on the 18-th Internat. Conference on High Energy Physics, Tbilisi 1976, CERN preprint CERN/EP/Phys. 76–56.

[12] J. Kripfganz, J. Ranft, CERN preprint TH 2244 (1976).

[13] S. M. Berman, J. D. Bjorken, J. B. Kogut, *Phys. Rev.* **D4**, 3388 (1971); J. D. Bjorken, *Phys. Rev.* **D8**, 4078 (1973).

[14] S. D. Ellis, M. B. Kislinger, *Phys. Rev.* **D9**, 2027 (1974).

[15] R. D. Field, R. P. Feynman, *Phys. Rev.* **D15**, 2590 (1977).

[16] R. C. Hwa, A. J. Spiessbach, M. J. Teper, *Phys. Rev. Lett.* **36**, 1418 (1976).

[17] E. Fischbach, G. W. Look, *Phys. Rev.* **D15**, 2576 (1977).

[18] R. Blankenbecler, S. J. Brodsky, J. Gunion, *Phys. Lett.* **42B**, 461 (1972); J. Gunion, S. J. Brodsky, R. Blankenbecler, *Phys. Rev.* **D6**, 2652 (1972).

[19] D. Sivers, S. Brodsky, R. Blankenbecler, *Phys. Rep.* **23**, 1 (1976).
[20] S. J. Brodsky, SLAC preprint, SLAC-Pub-1733, 1976.
[21] D. Schiff, A. P. Contogouris, J. L. Alonso, *Phys. Lett.* **55B**, 87 (1975).
[22] R. Raitio, G. Ringland, *Phys. Rev.* **D14**, 2291 (1976).
[23] R. Raitio, Wisconsin University preprint COO 545, 1976.
[24] P. V. Landshoff, J. C. Polkinghorne, *Phys. Rev.* **D8**, 4157 (1973); *Phys. Rev.* **D10**, 222 (1974).
[25] B. L. Combridge, *Phys. Lett.* **62B**, 222 (1976).
[26] J. D. Bjorken, Proceedings of the SLAC Summer Institute on Particle Physics 1975, SLAC-191, p. 85.
[27] S. D. Ellis, M. Jacob, P. V. Landshoff, *Nucl. Phys.* **B108**, 93 (1976).
[28] G. Ranft, J. Ranft, *Nucl. Phys.* **B110**, 493 (1976).
[29] W. Furmański, J. Wosiek, *Acta Phys. Pol.* **B8**, 633, 649 (1977).
[30] J. Gasser, U. P. Sukhatme, Cambridge preprint DAMPT 76-3, 1976.
[31] G. Preparata, G. Rossi, *Nucl. Phys.* **B111**, 111 (1976).
[32] M. Jacob, P. V. Landshoff, *Nucl. Phys.* **B113**, 395 (1976).
[33] J. Ranft, G. Ranft, *Acta Phys. Pol.* **B8**, 179 (1977).
[34] J. Ranft, G. Ranft, *Acta Phys. Pol.* **B8**, 275 (1977).
[35] R. Baier, J. Cleymans, K. Kinoshita, B. Petersson, *Nucl. Phys.* **B118**, 139 (1977).
[36] V. Matveev, R. Muradyan, A. Tavkhelidze, *Lett. Nuovo Cimento* **7**, 719 (1973).
[37] S. J. Brodsky, G. R. Farrar, *Phys. Rev. Lett.* **31**, 1153 (1973).
[38] R. McElhaney, S. F. Tuan, *Phys. Rev.* **D8**. 2267 (1973).
[39] V. Barger, R. J. N. Phillips, *Nucl. Phys.* **B73**, 269 (1974).
[40] R. Blankenbecler et al., SLAC preprint, SLAC-Pub 1513, 1975.
[41] G. R. Farrar, *Nucl. Phys.* **B17**, 429 (1974).
[42] G. Altarelli, N. Cabibbo, L. Maiani, R. Petronzio, *Nucl. Phys.* **69B**, 531 (1974).
[43] J. Okada, S. Pakvasa, S. F. Tuan, *Lett. Nuovo Cimento* **16**, 555 (1976).
[44] V. Barger, T. Weiler, R. J. N. Phillips, *Nucl. Phys.* **B102**, 439 (1976).
[45] R. E. Taylor, Proc. of the 1975 Int. Symp. on Lepton and Photon Interactions at High Energy, Stanford 1975, p. 679.
[46] D. C. Fetzer, H. Schlereth, Aachen preprint, 1976.
[47] P. V. Landshoff, preprint CERN-TH 2238, 1976.
[48] C. A. Heusch, Invited report to the Int. Neutrino Conference, 1976. Aachen, preprint UCSC 76–53.
[49] G. Hanzen, Contribution to VII-th Int. Colloquium on Multi-Particle Reactions, Tutzing–Munich, 1976.
[50] C. del Papa et al., preprint SLAC-Pub 1811, 1976.
[51] J. P. Berge et al., preprint Fermi-Lab PUB 75/84 Exp.; *Phys. Rev. Lett.*
[52] J. Kripfganz, to be published.